MESOSCALE AIR POLLUTION DISPERSION MODELS—I. EULERIAN GRID MODEL

N. D. van Egmond and H. Kesseboom

National Institute of Public Health, Bilthoven, The Netherlands

Abstract—To support the data interpretation of the dense air pollution monitoring network in The Netherlands, two numerical models were developed which describe the air pollution transport over the 400 km × 400 km area around the country. The models are designed for efficient, operational applications on a mini-computer system and require only limited sets of input data. The Eulerian GRID model, described in this paper, is based on the pseudo-spectral advection scheme for a 32 × 32 grid with a gridsize of 15 km. Vertical stratification in a surface, mixing and reservoir layer enables an adequate description of the temporal variability of concentrations. Spatial correlations between measured and modelled SO_2 concentrations are moderate. Some lack of correlation is ascribed to inaccuracies in foreign emission data rather than the degree of meteorological sophistication.

1. INTRODUCTION

In The Netherlands, being situated downwind of important European source areas, air pollution levels of SO_2, NO_2, NO and O_3 are measured continuously by a nationwide monitoring network covering an area of 200 km × 300 km. In order to interpret the measured annual mean SO_2 concentrations in terms of emissions, an earlier study (van Egmond *et al.*, 1979) was directed towards the estimation of fractional contributions of the nearby source areas by fitting mesoscale Gaussian plume profiles to the average concentrations measured per windspeed/wind-direction category. It was concluded that the foreign source areas contributed for about 65 % to the average SO_2 concentration over the country. However, exceedances of the proposed public health SO_2 standards have been observed for the 98-percentile threshold level of $250\,\mu g\,m^{-3}$ rather than for the 50-percentile level of $75\,\mu g\,m^{-3}$ (24 h values). In order to evaluate the contributions of pollution at the apparently more critical peak levels, two numerical models were developed for the description of SO_2 transport during episodes of higher pollution levels over the 400 km × 400 km area around of The Netherlands.

The retrospective models are designed for cost-efficient mini-computer application and directed to the limited set of input data which are measured on a routine basis by the monitoring network, i.e.

wind speed, wind direction and standard deviation of wind direction at 10 m level (hourly averages; 40 stations);

wind speed, direction and deviation at certain levels between 150 and 300 m at TV-towers;

solar radiation at 3 stations (hourly values) and

mixing height as measured by means of an acoustic sounder and occasionally, thermosonde ascents.
The models are expected to describe:

(i) The spatial variability of air pollution with the same or higher resolution as the monitoring network (20 km); in the major urban–industrial area resolution has to be increased to 3 km. (Apart from SO_2, the components NO_2, NO and O_3 are to be modelled by (later) implementation of chemical submodels.)

(ii) The major temporal variability as induced by the diurnal cycle in atmospheric stability and mixing height, resulting in increasing concentrations during the morning hours (fumigation).

These specifications cannot easily be met by one model. For applications with both high and low spatial resolutions at the same time for comparison of local contributions with mesoscale fluxes, a Lagrangian PUFF or segmented plume model is advantageous. Moreover these types of models have a high computational efficiency for relatively few sources. However, the inclusion of chemical reactions is limited to first-order transformation e.g. the oxidation of SO_2 to SO_4^{2-}. Modelling the transport of several reactive species like NO_2, NO and O_3 should be based on Eulerian GRID models as herein the "mixing" of several components can be simulated.

The requirements were met by developing both a Lagrangian PUFF and an Eulerian GRID model, which were based on the same treatment of the meteorological input data. In this paper the GRID model, including the underlying meteorology is presented. The PUFF model will be described in the accompanying paper (van Egmond and Kesseboom, 1983).

2. EMISSIONS

The models simulate the transport of SO_2, and in the case of the GRID model also SO_4^{2-} over the 400 km square around The Netherlands (Fig. 1). The
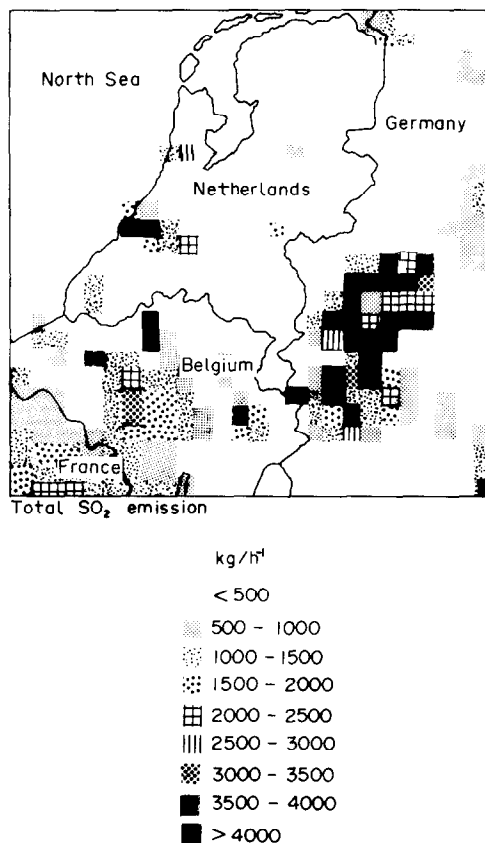
Fig. 1. SO_2 emissions in the 400 km × 400 km model area; total emission is 521 tons h⁻¹ excluding individual point sources in The Netherlands.

emissions are given for every grid square of 15 km side and grouped into three categories; sources with effective heights lower than 150 m, sources with effective heights over 150 m and individual point sources. The lower sources are given an effective height of 50 m and the higher sources of 375 m; total emissions are 385 T h⁻¹ and 136 T h⁻¹, respectively. The SO_2-emissions were obtained from an emission inventory of The Netherlands produced by TNO (1979) and for the other countries also based on the OECD–LRTAP study (1979). The emissions are not time, or temperature dependent. A detailed adjustment of the emission data by means of available transmission data from Cospec-remote sensing measurements is being prepared.

3. METEOROLOGY

3.1. General formulation and assumptions

Transport and dispersion of pollutants are assumed to take place in three atmospheric layers: a surface layer, a mixing layer and a reservoir layer. In contrast with the surface and reservoir layers, the height of the mixing layer is time dependent. Within the mixing and

reservoir layers the pollutants are assumed to be perfectly mixed, while in the ground-based surface layer an analytical concentration profile is assumed, resulting from the relative resistances to pollutant transport though the surface layer, the air–surface interface and the surface itself (dry deposition).

As such the dry deposition is modelled as a time-varying function of both aerodynamic and surface resistances. These resistances are derived from the surface layer characteristics which, in turn, are obtained from measured wind speed and radiation data (dry deposition). The vertical structure and dry deposition are assumed to be constant throughout the area, which is expected to be justified for the topographical structure of the area of application.

The vertical stratification, time variability of mixing height and typical concentration profile are presented in Fig. 2.
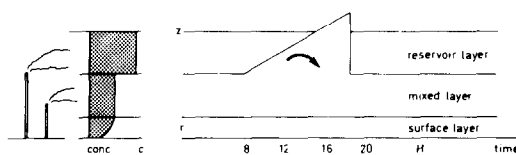

Fig. 2. Vertical stratification in surface, mixing and reservoir layer and diurnal variation of mixing height.

(a) In the mixing layer a uniform concentration distribution is assumed, excluding the lowest 50 m (surface layer). The time-dependent height of the mixing layer is obtained from acoustic sounder measurements and thus defined as the level at which strong temperature gradients occur, i.e. inversion height. During episodes the sounder data are supplemented by the results of thermosonde ascents.

In cases where no measurements are available an estimate for the initial mixing height is given by the diagnostic expression for the early morning stable boundary layer height $h(m)$

$$h = 2400\, u_*^{3/2} \qquad (1)$$

as obtained by Venkatram (1980) by simplification of the Zilitinkevich (1972) expression, where friction velocity u_* (m s⁻¹) is derived from wind speed and radiation measurements. However, this boundary layer height is defined as the height of the stable Ekman-boundary layer, which is not necessarily identical to inversion height. Given the retrospective character of the model, this height nevertheless can be used as a first estimate for the initial mixing height.

(b) The surface layer is defined as the lowest 50 m of the mixing layer. In this layer the profiles of wind speed, turbulent diffusion and concentration are strongly determined by the interaction with the surface. The introduction of a surface layer enables modeling of dry deposition and the resulting concentration gradient near ground level, as a function of time

dependent atmospheric stability. The relevant aerodynamic resistances are derived from the surface layer characteristics u_* and Obukhov length L, which in turn are deduced from hourly windspeed and radiation data. The values of u_* and L are assumed to be constant throughout the area.

(c) The reservoir layer is defined as the layer above the mixing height in which pollutants are emitted by high sources. During the morning hours the mixing height increases due to the incoming solar heat flux and pollutants from the reservoir layer are transported proportionally to the mixing layer, which results in increasing mixing layer concentrations (fumigation) when reservoir concentrations are relatively high. The depth of the reservoir layer is, thus, defined by the initial height of the mixing layer and the time the fumigation ends, which in the present case of a retrospective model, can easily be derived from concentration measurements. In the example of Fig. 2, fumigation ends at 14.00 h; after this time no reservoir layer is modelled and all pollutants are emitted into the expanding volume of the mixing layer, generally resulting in a decrease of concentrations. The top of the reservoir layer ranges in most cases between 300 and 700 m. At the end of the afternoon, the heat flux becomes negative and through an undefined stabilization process, the stratification in the mixing and reservoir layer is restored. At the same time the surface layer resistance to pollution is increased, accompanied with an associated change in surface layer-concentration profile. As such, the major diurnal variability in ground level concentrations is accounted for by the model.

Wind fields are constructed for mixing and reservoir layer separately and are derived from hourly measurements at various levels. The two-dimensional fields are non-divergent.

Horizontal turbulent diffusion K_H is assumed to be constant over the area. In the GRID model K_H is also constant in time and, given the spatial resolution of the grid (15 km) rather insignificant. In most applications K_H was chosen to be zero, which also strongly benefits computation time. In the PUFF model K_H is a time-dependent function of the standard deviation of the horizontal wind components, as horizontal diffusion is more relevant at the higher spatial resolution of the PUFF model.

Oxidation of SO_2 to SO_4^{2-} is modelled as a first order reaction, dependent on the (measured) solar radiation. The decay rate is assumed to be constant throughout the area.

3.2. Surface layer, dry deposition

The surface layer is defined as the layer in which the vertical turbulent diffusion K_z is limited by interaction of the earth surface. The height of the layer is normally defined by the absolute value of the stability dependent Obukhov length L. In this study, where the category of low sources has effective heights of 50 m, the surface layer is assumed to have a constant height $z = 50$ m.

Dry deposition at the surface generates a height independent flux F through this layer:

$$F = K(z)\frac{dC(z)}{dz} = v_g(z)C(z). \qquad (2)$$

As the turbulent diffusion $K(z)$ decreases at decreasing height z, the resulting concentration profile has the strongest gradient near ground level. In a preceding study by van Dop et al. (1980) the quasi-stationary SO_2 concentration profile, measured at a 200 m meteorological tower, could be fully explained by mesoscale advection and dry deposition.

For the model computations dry deposition is obtained as

$$v_g = (r_a + r_s + r_c)^{-1} \qquad (3)$$

where (i) aerodynamical resistance $r_a = \int_0^{50} K(z)^{-1} dz$.

Given the $K(z)$ profile for the surface layer (Businger, 1973) the r_a profile is found by integration (Weseley and Hicks, 1977):

$$r_a = (ku_*)^{-1}(\ln z/z_0 - \phi_c). \qquad (4)$$

The stability correction ϕ_c is given by

$$\phi_c = \exp(0.598 + 0.39\ln(-z/L) - 0.09[\ln(-z/L)]^2)$$

for $L < 0$ (unstable)

and

$$\phi = -5z/L \quad \text{for} \quad L > 0 \text{ (stable)}$$

with roughness length $z_0 = 0.05$ m, $z = 50$ m and $k = 0.35$.

(ii) Surface resistance $r_s = 2.6(ku_*)^{-1}$ and

(iii) canopy resistance r_c, estimated at 70 s m^{-1} (Fowler, 1978).

When the three resistances are computed from the Obukhov length L and friction velocity u_*, both the deposition velocity and the shape of the concentration profile over the surface layer can be established. The concentration at the (measurement) level of 4 m, $C(4)$ is related to the concentration $C(50)$ at the top of the surface layer, as the fluxes $F = v_g C$ are assumed to be constant over the layer and thus the same at both levels. From (2) and (3)

$$C(4) = C(50)(r_c + r_s + r_{a4})/(r_c + r_s + r_{a50}) \qquad (5)$$

r_{a4} and r_{a50} are the aerodynamical resistances over the lowest 4 and 50 m, respectively. In the model, the 4 m-concentrations are obtained as the mixing layer concentration $C(50)$, times the ratio $C(4)/C(50)$. So the numerical advection scheme only deals with the mixing and reservoir layers, while the surface layer is treated analytically as a pseudo-layer, with the consequent reduction in computation time.

3.3. Computation of L and u_*

The Obukhov length L and friction velocity u_*, characteristic for the surface layer stability and transport resistances, are derived for every simulation hour from measured spatial average 10 m windspeed and spatial average solar radiation H. As no data are

available for direct calculation of the sensible heat flux H_0, stable (night) and unstable conditions (day) are treated separately.

During daytime it is assumed that: (i) albedo a = 0.20 for average conditions and a = 0.80 in case of snow cover and (ii) 20% of the remaining radiation is entrained in the mixing layer as sensible heat flux H_0:

$$H_0 = 0.20(1 - a)H. \qquad (6)$$

Albedo a is a model-input parameter so that corrections to this simplification can be made during model applications.

Given the surface layer wind profile (Businger, 1973)

$$u(z) = \frac{u_*}{k}(\ln(z/z_0) - \Psi(z/L)) \qquad (7)$$

with

$$\Psi(z/L) = 2\ln((1 + x)/2) + \ln((1 + x^2)/2)$$
$$- 2\operatorname{arctg}x + \pi/2$$

with $x = (1 - 15z/L)^{\frac{1}{4}}$ and $L < 0$ for the neutral and unstable conditions, together with the definition of Obukhov length

$$L = -\rho c_p T_0 u_*^3/k g H_0 = -91 u_*^3/H_0,$$

the values of L and u_* can be computed iteratively from H_0 and 10 m windspeed.

For stable conditions, at which $L > 0$, occurring at low or zero radiation levels, the empirical relation of Venkatram (1980) can be applied

$$L = 1100 u_*^2 \qquad (8)$$

and u_* can be computed directly from the 10 m windspeed, as for stable conditions

$$\Psi(z/L) = -5z/L.$$

The diurnal profiles of v_g at the reference height of 50 m, for several values of albedo, are given in Fig. 3. At larger albedo values, stability increases and dry de-

position is reduced. The sensitivity of v_g for variations in albedo, and thus for assumed constants in the computation of H_0, is moderate.

3.4. Windfields

For the numerical advection in the mixing and reservoir layer, representative windfields have to be derived from the measured 10 m winds at 40 stations and winds at levels between 150 and 300 m at 5 TV-towers. Wind direction, speed and standard deviation of wind direction are obtained as hourly average values. Winds at higher levels (e.g. 850 mb) are not available within the operational framework of the network and were not considered, although this might result in misinterpretation at elevated inversions.

For the interpolation of windspeeds at heights beyond the extension of the surface layer the exponents p of the power law profile

$$u(z) = u(10)(z/10)^p \qquad (9)$$

are computed from the measured winds at 10 m, $u(10)$ and at elevated levels $u(z)$. For all 40 meteorological stations measuring winds near ground level, winds at the heights of the mixing and reservoir layer are computed from the spatial average exponent $\langle p \rangle$. During daytime $\langle p \rangle$ was found to be about 0.10 while at nocturnal, stable conditions $\langle p \rangle$ increased to about 0.60.

Interpolation of wind direction is based on the Ekman–Taylor spiral-windprofile, assuming a height independent "bulk" turbulent diffusivity K_{zm}. The angle $\alpha(z)$ between the wind at height z and the geostrophic wind is given by

$$\alpha(z) = \sin(zq)/(e^{zq} - \cos(zq)) \qquad (10)$$

with $q = \sqrt{\lambda/2K_{zm}}$ where λ the Coriolis parameter.

At the 5 TV-towers and the nearby 10-m stations, the difference $\alpha(z) - \alpha(10)$ is measured from which K_{zm} is computed numerically. Just as for wind speed
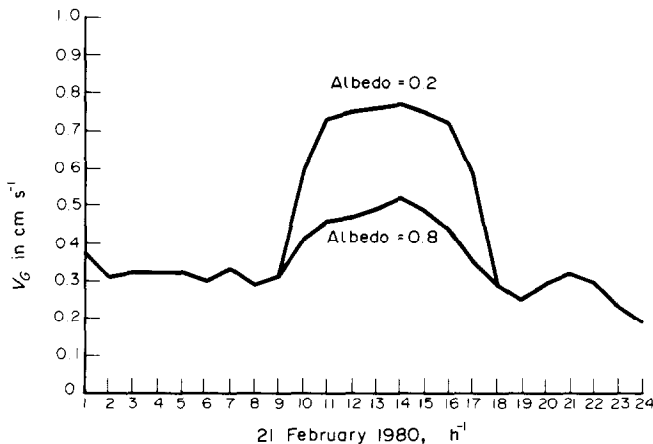

Fig. 3. Deposition velocity profile at reference height $z = 50$ m, for several values of surface albedo, for 21 February 1980.

interpolation, the directions at representative heights for the mixing and reservoir layer are computed at all 40 meteorological stations from the spatial mean $\langle K_{zm} \rangle$. In Fig. 4 the diurnal profile of K_{zm} at 21 February 1980 is compared with the values of $K(z)$ as computed from the surface layer K-profile, as given by Businger (1973):

$$K(z) = \frac{k u_* z}{\phi_h} \quad (11)$$

with $\phi_h = 0.74 (1 - 9z/L)^{-0.5}$ for $L < 0$ (unstable)
$\phi_h = 0.74 + 4.7 z/L$ for $L > 0$ (stable).

The diurnal profile of K (50), at the top of the surface layer, is strongly determined by the diurnal profile of solar radiation from which the profile of L is derived as described above. The profile of "bulk" $\langle K_{zm} \rangle$, derived from wind measurements according to Equation (10) gives a more realistic description of the turbulent diffusivity in the mixing layer.

Horizontal interpolation from the 40 meteo-stations to the 32 × 32 grid points over the 400 km side area is achieved by a negative exponential weighting scheme for individual u and v components. The grid point value u_0 is obtained as a linear combination of the wind components u_i at the 40 stations:

$$u_0 = \sum_{i=1}^{N} f_i u_i, \quad N = 40$$

with

$$f_i = \frac{e^{-x_i/R}}{\sum_{i=1}^{N} e^{-x_i/R}} \quad (12)$$

where x_i is the distance between grid point and station i, R is a specific spatial (correlation) distance.

As the wind fields have to be mass-consistent the divergence

$$D = \frac{\partial u}{\partial x} + \frac{\partial v}{\partial y}$$

is reduced at all field positions to values less than $1 \times 10^{-6} \text{s}^{-1}$ by the iterative method given by Endlich (1967).

3.5. Numerical advection

Transport and diffusion is simulated by integration of the two-dimensional continuity equation in each layer separately

$$\frac{\partial C}{\partial t} = \left(u \frac{\partial C}{\partial x} + u \frac{\partial C}{\partial y} \right) + K_H \left(\frac{\partial^2 C}{\partial x^2} + \frac{\partial^2 C}{\partial y^2} \right) + Q_c - S_d - S_c \quad (13)$$

where K_H is the horizontal diffusivity; Q_c, concentration change resulting from emission; S_d, dry deposition; $S_d = -\frac{v_g}{h_m} C$, with h_m the height of the mixing layer and C the mixing layer concentration; in the reservoir layer $S_d = 0$ and S_c, scavenging of SO_2 by oxidation to SO_4 given by $S_c = -(c_1 + c_2 H)C$. The constant c_1 is set to 0.01 h^{-1} for c_2 the value

given by Gillani (1978) is adopted; $c_2 = 0.032 \text{h}^{-1} \text{m}^{-2} \text{kW}^{-1}$.

Numerical advection over the 32 × 32 grid with grid distances of 15 km is based on the pseudo-spectral scheme given by Christensen and Prahm (1976). De Haan (1980) demonstrated that this scheme has a high accuracy, hardly generates pseudo-diffusion and requires only modest computation time.

The gradients $\partial C/\partial x$ are $\partial C/\partial y$ are determined separately for x- and y-directions by writing

$$C(x) = \sum_k A(k) \exp\left(j 2\pi \frac{k}{N \Delta x} x \right) \quad (14)$$

with $A(k)$ the Fourier components for wave numbers $k/N\Delta x$; $\Delta x = 15$ km grid distance and $N = 32$, number of grid points in one dimension.

The derivatives are easily found as:

$$\frac{\partial C(x)}{\partial x} = \sum_k j 2\pi \frac{k}{N \Delta x} A(k) \exp\left(j 2\pi \frac{k}{N \Delta x} x \right). \quad (15)$$

The second derivative is found by a second multiplication with coefficients $j 2\pi k/N\Delta x$.

So for every line of grid points $C(x)$ the spectral representation $A(k)$ is computed by means of the Fast Fourier Transform method (Cooly and Tukey, 1965). After multiplication with the wave number dependent coefficients the derivative profile is obtained by inverse transformation. This implies that for every time step and every layer 32 × 32 × 2 FFT's have to be made for first order derivatives. For $K_H \neq 0$, 32 × 32 extra inverse transformations are required. At time steps of 6 min, two transport-layers and one component (SO_2), the simulation of 1-h advection, requires 3840 Fast Fourier Transforms.

In order to account for the periodic boundary conditions which are inherent with the spectral representation of $C(x)$ by $A(k)$, the gradients at the boundaries of the field have to be small, i.e. no pollution is allowed to be transported out of the field. To achieve this in a practical way, an additional decay term over the outer 3 grid-rows is introduced reducing the pollution flux to zero over the transport distance of $3\Delta x = 45$ km.

Spatial fluctuations with wave numbers higher than $1/2\Delta x$ are folded back to lower numbers in the spectral representation $A(k)$. This "aliasing" effect results in errors in the derivatives. To account for this bias, once in the 18–36 time steps a Lanczos-Sigma filtering is applied to the field. The filtered concentration profile is given by

$$C(x) = \sum_k \frac{\sin(2\pi k/N)}{2\pi k/N} A(k) \exp\left(j 2\pi \frac{k}{N \Delta x} x \right). \quad (16)$$

The filter is found to be very effective in bias reduction.

Time integration is performed by the leap-frog scheme:

$$C_{t+1} = C_{t-1} + 2\Delta t \left(\frac{\partial C}{\partial t} \right)_t, \quad (17)$$

with $\left(\dfrac{\partial C}{\partial t}\right)_t$ the concentration change estimated at time
t. For $K_H \neq 0$ this integration scheme formally is not stable. However in the present application the numerical instability could be adequately suppressed by the Sigma filter. Time steps were chosen such that the advection distance is limited to $1/5$ grid-cell per time step.

5. COMPUTATIONAL ASPECTS

The GRID model is designed to run on a mini-computer system. For the present applications a Hewlett packard 1000 F-system under RTE IV was used. The GRID program consists of three segments: main program 22 K bytes; advection segment 30 K bytes; meteorological segment 10 K bytes, and additional array-memory of 80 K bytes, defined under EMA. In memory, space has to be reserved for the main program and the largest segment (52 K bytes).

Computation time in average conditions amounts 240 CPU-seconds for one simulation hour.

Apart from wind and radiation data, the set of input parameters is limited to initial mixing height, rising speed of mixing height, start and end of fumigation period, hour of afternoon stabilization, albedo and K_H: these parameters are read interactively from a CRT-terminal.

6. SENSITIVITY ANALYSIS

The sensitivity of the model results for changes in the relevant input parameters was evaluated from the concentration levels at the end of the fumigation period (14.00 h), resulting from one hour emission before the fumigation started (8.00 h). So the effect of input change is measured over the full fumigation cycle. The meteorology of 21 February 1980 was used as a representative reference set.

(a) Horizontal diffusivity K_H only resulted in a concentration change at $K_H > 10{,}000\,\mathrm{m^2\,s^{-1}}$. At $K_H = 30{,}000\,\mathrm{m^2\,s^{-1}}$ the concentration maximum decreased with 22 % for low sources, and with 15 % for high sources. As expected the horizontal diffusivity is not overly important at the grid size of 15 km.

(b) The resistance r_c was changed from 70 to $100\,\mathrm{s\,m^{-1}}$, resulting in a concentration increase of 11 % for low, and 8 % for high (reservoir layer) sources.

(c) Albedo increase of $a = 0.2$ to $a = 0.8$ in Equation (6) resulted in a 16 % decrease for low sources. The associated increase in stability leads to a lower ground level concentration (-23 %) due to the increased resistance over the surface layer and a lower $C(4)/C(50)$ ratio as given by Equation (5). On the other hand the decreased dry deposition results in an increased concentration level ($+7$ %) after 6 h of transport. The net result is a concentration decrease of 16 %. The dependence of dry deposition on albedo,

and consequently other factors in the solar radiation–sensible heat flux scheme, are presented in Fig. 3.

(d) Wind change was simulated by reducing the mixing layer/surface layer reference height for the computation of the wind field by vertical interpolation from 70 to 50 m. A subsequent concentration increase of 4 % was observed.

(e) Mixing height was increased from 200 m as initial height to 250 m at unchanged rising speed of $20\,\mathrm{m\,s^{-1}}$. This resulted in a concentration decrease of 7 % for low (mixing layer) and 9 % for high (reservoir layer) sources.

(f) Source height changes are only relevant as far as the emission is allocated to the reservoir layer instead of the mixing layer and vice versa. At the mixing height of 200 m this resulted in a concentration change of 10 % after the fumigation period. It will be clear that the effect will be almost 100 % during the hours before fumigation starts.

Numerical mass consistency was tested by diagonal transport over the grid. At a homogeneous wind field the mass changes were less than 1 %; at measured wind fields, errors up to 2 % were observed resulting from non-eliminated divergence.

7. CASE STUDY: 20 AND 21 FEBRUARY 1980

The performance of the grid-model is demonstrated for 20 and 21 February 1980. This period is representative for general situations in which an anti-cyclonic circulation transports pollution from a major source area, the German Ruhr district (see Fig. 1) into The Netherlands. In 1979 such mesoscale transports resulted in exceedances of the 98 %-threshold level of $250\,\mu\mathrm{g\,m^{-3}}$ for daily average SO_2 concentrations as advised by the National Health Council.

At 20 and 21 February the general circulation was dominated by an anti-cyclone over the U.S.S.R., resulting in a south-easterly wind of 3–$5\,\mathrm{m\,s^{-1}}$ at ground level. Temperature ranged from $0°C$ at night to $8°C$ in the afternoon with cloudless sky. Mixing height, as measured by means of an acoustic sounder indicated an initial mixing height of 175 m and an increase of this
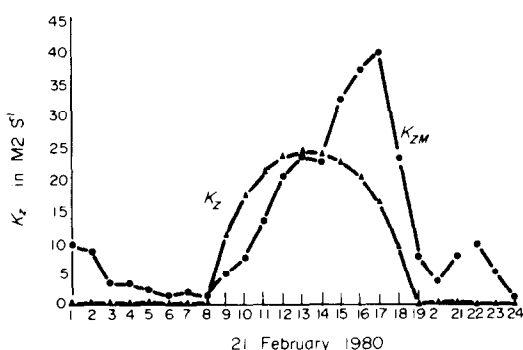

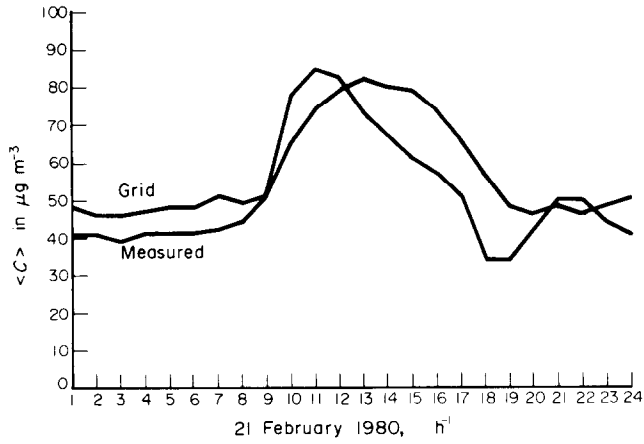Fig. 4. Profiles of $\langle K_{zm} \rangle$ and $K_z(50)$ at 21 February 1980.

Fif. 5. Diurnal profiles of measured and modelled spatial mean SO_2 concentration over The Netherlands at 21 February 1980.
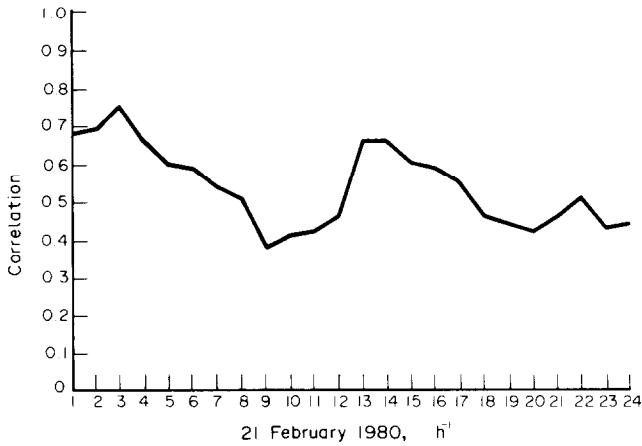

Fig. 6. Diurnal profile of correlation between measured and modelled SO_2 concentrations for 100 monitoring stations over The Netherlands at 21 February 1980.
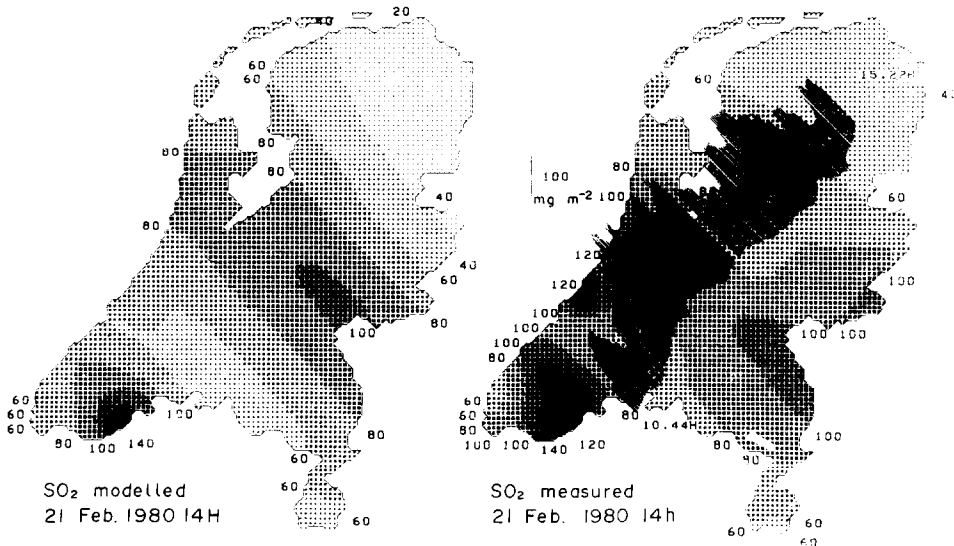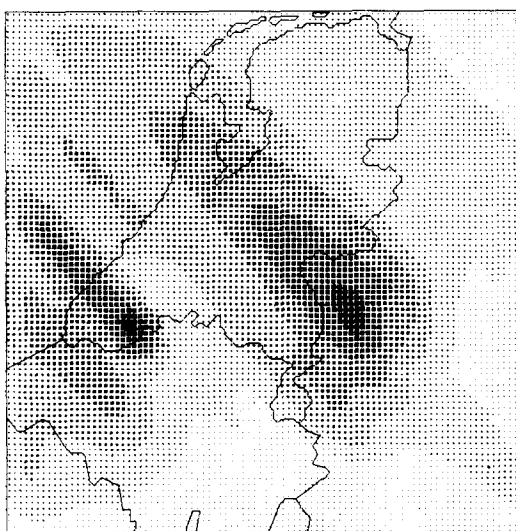

SO₂ modelled
21 Feb. 1980 14H

SO₂ measured
21 Feb. 1980 14h

Fig. 7. Measured and modelled SO_2 concentration fields in $\mu g\ m^{-3}$ and measured SO_2 gasburden profile at 21 February 1980.

height with $20\,\mathrm{m\,h^{-1}}$ to about $400\,\mathrm{m}$ at $16.00\,\mathrm{h}$. According to the diagnostic Equation (1), mixing height was estimated as $180\,\mathrm{m}$ at $7.00\,\mathrm{h}$. Fumigation ended at about $13.00\,\mathrm{h}$. From these data the diurnal profile of vertical stratification, as given in Fig. 2, is defined.

The diurnal profiles of $\langle K_{zm} \rangle$ and $K_z(50)$ were already given in Fig. 4. The profiles of measured and modelled spatial mean concentration in The Netherlands are presented in Fig. 5. The modelled profile agrees qualitatively with the measured profile; however the increase of concentration during fumiga-

tion between $9.00\,\mathrm{h}$ and $13.00\,\mathrm{h}$ occurs too rapidly in the model, which is explained by the rapid increase of $K_z(50)$. As demonstrated by the $\langle K_{zm} \rangle$ profile, the time delay in the sequence radiation–sensible heat flux–vertical turbulence has to be taken into account The spatial correlations between measured and modelled concentrations are presented in Fig. 6; they are poor, especially during fumigation. However detailed analysis of these correlations indicated that the major discrepancies occur at the borders near the foreign source areas and are ascribed to inaccuracies in the emission data. Moreover the concentrations within the
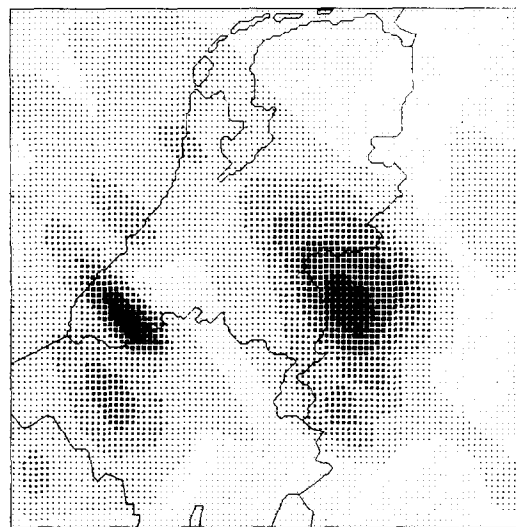

SO2 21 FEB 1980 7 UUR (GRID -MODEL)
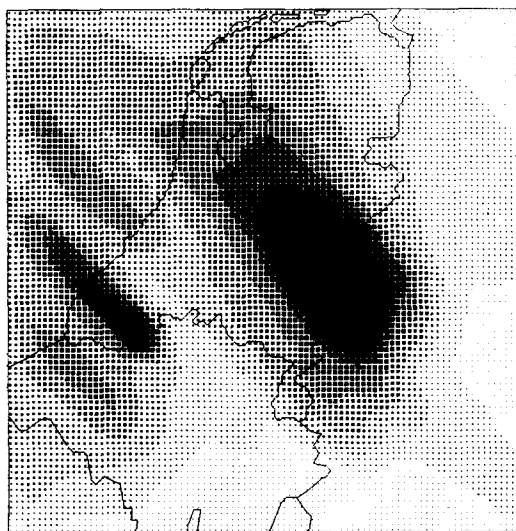
SO2 21 FEB 1980 10 UUR (GRID -MODEL)
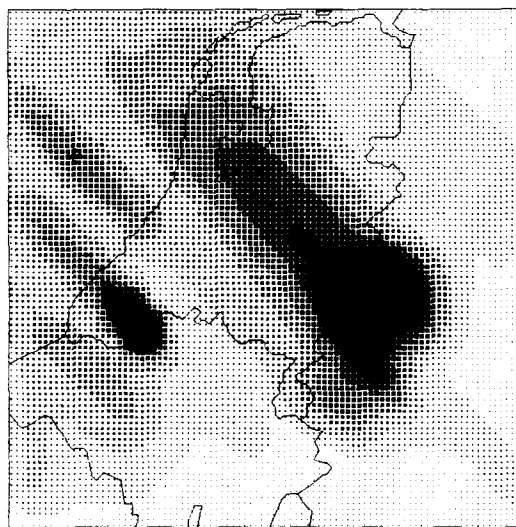
SO2 21 FEB 1980 14 UUR (GRID -MODEL)
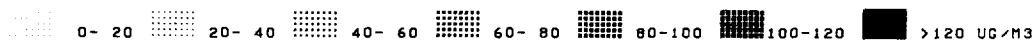
SO2 21 FEB 1980 18 UUR (GRID -MODEL)

0- 20   20- 40   40- 60   60- 80   80-100   100-120   >120 UG/M3

Fig. 8. Modelled SO_2 concentration at 21 February 1980 for the $400\,\mathrm{km} \times 400\,\mathrm{km}$ model area.

Dutch Rotterdam–Rijnmond source area were not modelled properly. The initial mixing over the 15 km × 15 km boxes results in concentrations being too low. A superimposed Gaussian type model should have been used to avoid this structural effect. The discrepancies between measured and modelled fields within The Netherlands are presented in Fig. 7; herein also the gasburden profile, measured with a Cospec IV SO$_2$ remote sensor, is plotted. The secondary zone of higher gasburden levels to the north is explained from directional wind shear. As can be seen from the overall modelled concentration fields in Fig. 8, the transport zone of higher concentrations is shifted to the north during fumigation; the mesoscale plume in the reservoir layer is transported with a veered wind and broadens the plume zone when mixed downwards.

8. DISCUSSION AND CONCLUSION

The case study described above demonstrates that a typical diurnal air pollution pattern over The Netherlands can be described quantitatively by the simplified numerical mesoscale model presented here. Comparable model performance was observed in several other case studies of pollutant transport at different weather types. The discrepancies between modelled and measured concentrations were mainly due to inaccuracies in the emission data and failure to model sub grid scale plumes. Consequently, an improvement of the emission inventory is expected to be more relevant than a further sophistication of meteorology. For the intended routine applications, detailed meteorological information is generally not available and the degree of sophistication should be consistent with the available input data. The simplified vertical structure of only three layers appears to be adequate for a satisfying description of the concentration variability in space and time. Nevertheless the derivation of the minimum early morning mixing depth and, in particular, the maximum height in the afternoon should be refined, as in many cases the inversion heights go beyond the detection limits of the acoustic sounder. Although thermosonde data can supplement the missing information, the introduction of a simplified mixing height model, based on the integrated heat input, should be considered. By deriving the height of the reservoir layer from plume rise estimates, the *a priori* information from concentration measurements (time fumigation ends) could be further reduced without extension of the limited set of routinely available input data.

The analytical treatment of the surface layer is of great advantage with respect to computation time and favours the intended operational use of the model. However, it implies that all emissions are instantaneously mixed throughout the mixing layer and

moreover subjected to the deposition induced gradient over the surface layer (50 m). In the present application, this gives no significant errors for low level sources as almost all SO$_2$ sources within the test area (The Netherlands) are effectively higher than 50 m, due to the nationwide use of low sulfur natural gas for domestic heating. Large elevated sources should be modelled separately using a suitable Gaussian model. The foreign low level emission will be mixed throughout the vertical extent of the mixing layer before entering the test-area. For intended application of the model in NO$_2$ studies the surface layer is treated as a separate, third transport layer to account for the substantial low level, traffic NO$_x$ emissions.

REFERENCES

Businger J. A. (1973) In: *Workshop on Micrometeorology* (Edited by Haugen D. A.) Atm. Met. Soc.

Cooly J. W. and Tukey J. W. (1965) An algorithm for the machine calculation of complex Fourier series. *Maths Comput.* **19**, 297–301.

Christensen O. and Prahm L. P. (1976) A pseudo spectral model for dispersion of atmospheric pollutants. *J. appl. Met.* **15**, 1284–1294.

van Dop H., de Ridder T. B., den Tonkelaar J. F. and van Egmond N. D. (1980) Sulphur dioxide measurements on the 213 metre tower at Cabauw, The Netherlands. *Atmospheric Environment* **14**, 933–945.

van Egmond N. D. and Kesseboom H. (1983) Mesoscale air pollution dispersion models—II. Lagrangian PUFF model. *Atmospheric Environment* **17**, 267–274.

van Egmond N. D., Tissing O. and Kesseboom H. (1979) Estimating contributions of source areas to the measured yearly average SO$_2$-concentrations in the Netherlands by dispersion-model parameter optimization. *Atmospheric Environment* **13**, 1551–1557.

Endlich R. M. (1967) An iterative method for altering the kinematic properties of wind fields. *J appl. Met.* **6**, 837–844.

Fowler D. (1978) Dry deposition on agricultural crops. *Atmospheric Environment* **12**, 369–373.

Gillani N. V. (1978) Project MISST: Mesoscale plume modelling of the dispersion, transformation and ground removal of SO$_2$. *Atmospheric Environment* **12**, 569–588.

de Haan B. J. (1980) A comparison of finite difference schemes describing the two dimensional advection equation. *Proc. 11th Int. Techn. Meeting on Air Pollut. Mod. and its Appl.*, NATO–CCMS, Amsterdam.

OECD–LRTAP (1979) OECD, 2 rue André Pascal, 75775 Paris Cedex 16, France.

TNO, Rekensysteem Luchtverontreiniging II (1979) Schoenmakerstraat, Delft, Netherlands.

Venkatram A. (1980) Estimating the Monin–Obukhov length in the stable boundary layer for dispersion calculations. *Boundary-Layer Met.* **19**, 481–485.

Weseley M. L. and Hicks B. B. (1977) Some factors that effect the deposition rates of sulphur dioxide and similar gases on vegetation. *J. Air Pollut. Control Ass.* **27**, 1110–1116.

Zilitinkevich S. S. (1972) On the determination of the height of the Ekman boundary layer. *Boundary-Layer Met.* **3**, 141–145.